THEMIS Observations of Unusual Bow Shock Motion Attending a Transient Magnetospheric Event

G. I. Korotova
IZMIRAN, Troitsk, Moscow Region, 142190, Russia,
also at IPST/UMD, College Park, MD, 20742, USA

D. G. Sibeck
Code 674, NASA/GSFC, Greenbelt, MD 20771, USA

N. Omidi
Solana Scientific Inc., Solana Beach, CA, 92075, USA

V. Angelopoulos
IGPP/ESS, UCLA, Los Angeles, CA, 90095, USA

Abstract

We present a multipoint case study of solar wind and magnetospheric observations during a transient magnetospheric compression at 2319 UT on October 15,

2008. We use high-time resolution magnetic field and plasma data from the THEMIS and GOES-11/12 spacecraft to show that this transient event corresponded to an abrupt rotation in the IMF orientation, a change in the location of the foreshock, and transient outward bow shock motion. We employ results from a global hybrid code model to reconcile the observations indicating transient inward magnetopause motion with the outward bow shock motion.

1. Introduction

The interaction of interplanetary discontinuities with the Earth's bow shock and magnetopause has been the subject of intense research for many years. A host of observational studies have demonstrated that both boundaries lie nearer Earth during intervals of enhanced solar wind dynamic pressure (and magnetosonic Mach number) [e.g., Fairfield, 1971; Shue et al., 1997; Merka et al., 2005]. Working within the magnetohydrodynamic (MHD) framework, Volk and Auer [1974], **Wu et al. [1993], Cable and Lin [1998],** and Samsonov et al. [2007] showed that the interaction of an interplanetary discontinuity marked by a density/dynamic pressure increase with the bow shock launches the full set of forward and reverse fast, slow, and intermediate mode waves into the magnetosheath. The fast forward wave propagates through the magnetosheath and strikes the magnetopause. Here it launches another fast forward mode wave into the magnetosphere and the magnetopause moves inward. The fast reverse wave becomes the new bow shock, which also moves Earthward. These results lead one to expect a step function increase in the solar wind dynamic pressure to **initiate**

47 **abrupt** inward motion of the bow shock and magnetopause, as well as an **abrupt**
48 increase in the magnetospheric magnetic field strength and pressure.

49 **There have also been many observational studies concerning the response of**
50 **the bow shock, magnetopause, and magnetosphere to varying solar wind conditions.**
51 **Zhang et al. [2009] employed THEMIS observations to time the decelerating inward**
52 **motion of the bow shock, magnetopause, and transmitted discontinuities that**
53 **occurred in response to the arrival of an interplanetary shock. Safrankova et al.**
54 **[2007] showed that the bow shock rebounds following abrupt changes in its location.**
55 **Koval et al. [2005; 2006], Keika et al. [2009], Andreeva et al. [2011], and Volwerk et**
56 **al. [2011] presented results from numerical simulations and observations indicating**
57 **that interplanetary shocks deform upon encountering the bow shock to become**
58 **concave discontinuities that slow down and engulf the magnetosphere as they pass**
59 **through the magnetosheath. Nemecek et al. [2011] and Andreeva et al. [2011]**
60 **presented evidence for the faster antisunward propagation of the transmitted**
61 **disturbances through the magnetosphere than in the solar wind itself.**

62 Results from hybrid code simulations suggest that this simple picture sometimes
63 needs modification. They indicate that hot flow anomalies accompany the interaction of
64 some interplanetary magnetic field (IMF) discontinuities with the bow shock [Omidi and
65 Sibeck, 2007]. Hot flow anomalies lie centered on the discontinuities upstream from the
66 point where they intersect the bow shock. They are bounded by shocks that also extend
67 upstream from the Earth's bow shock, and exhibit greatly heated and deflected solar wind
68 plasmas. Bundles of IMF field lines connected to the bow shock often excavate cavities
69 of depressed magnetic field strength and density bounded by compressional boundaries in

the region upstream from the bow shock, but exhibit no shocks, heated plasmas, or deflected flows [Omidi et al., 2009]. **The signatures of hot flow anomalies and foreshock cavities have been seen in the magnetosheath, and the corresponding pressure variations may cause large amplitude magnetopause motion and perturbations of the magnetospheric magnetic field [Paschmann et al., 1988; Sibeck et al., 1999].**

Transient (1-10 min duration) magnetic field and plasma events are common in the vicinity of the dayside magnetopause. They have been attributed to boundary waves driven by solar wind dynamic pressure variations [e.g., Sibeck et al., 1989], unsteady magnetopause merging and the generation of flux transfer events (FTEs) [e.g., Russell and Elphic, 1978], the Kelvin-Helmholtz (KH) instability [e.g., Southwood, 1979] and impulsive plasma penetration [e.g., Lemaire, 1977]. Korotova et al. [2011] showed that one such transient event observed at the magnetopause with FTE characteristics was in fact produced by the interaction of the solar wind and bow shock when a complicated sequence of varying IMF directions and solar wind pressures created significant effects, including inward bow shock and magnetopause motion, compressions of the magnetosphere, and the transient event itself.

In this paper we present a multipoint THEMIS case study of a transient event with FTE-like bipolar Bn signatures in the direction normal to the magnetopause observed just inside the pre-noon magnetopause at ~2319 UT on October 15, 2008. Observations indicate that this event was associated with a single transient outward motion of the bow shock. We use a global hybrid code model to explain the observations, demonstrating that an IMF tangential discontinuity launches the pressure pulse that

93 triggers both the transient magnetospheric event and the unusual outward bow shock
94 motion.
95
96 **2. Data sets, spacecraft, orbits**
97 The five THEMIS spacecraft carry identical instruments. The ESA electrostatic
98 analyzer on each THEMIS spacecraft measures the distribution functions of 0.005 to 25
99 keV ions and 0.005 to 30 keV electrons over 4π steradian, providing accurate high time
100 resolution plasma moments, pitch angle and gyrophase particle distributions as often as
101 each 3s. [McFadden et al., 2008]. The FGM triaxial fluxgate magnetometer measures the
102 background magnetic field and its low frequency fluctuations up to 64 Hz [Auster et al.,
103 2008]. The spacecraft return magnetic field vectors, omnidirectional particle spectra, and
104 plasma moments computed on-board once every 3s throughout their orbit. We compare
105 the THEMIS observations with 0.5s time resolution GOES geosynchronous magnetic
106 field observations [Singer et al., 1996].
107
108 3**. Spacecraft observations**
109 Figure 1 shows the locations of five THEMIS and GOES 11 and 12 spacecraft from
110 2230 to 2400 UT on October 15, 2008. THEMIS A, D and E moved through the pre-noon
111 magnetosphere outbound from GSM (X, Y, Z) = (6.72, -7.83, -1.91) R_E to (7.78, -7.55, -
112 1.76) R_E and inbound from (8.59, -1.87, 0.32) R_E to (7.92, -1.01, 0.45) R_E and from (8.86,
113 -2.28, 0.25) R_E to (7.68, -0.75, 0.49) R_E, respectively. THEMIS B and C were
114 nominally in the solar wind just outside the pre-noon bow shock, moving from GSM (X,
115 Y, Z) =(4.37, -22.50, -4.01) R_E to (5.00, -23.34, -3.66) R_E and from (10.63, -16.22, -1.52)

R_E to (11.12, -16.00, -1.21) R_E, respectively. The location and shape of the magnetopause have been taken from the empirical study of Roelof and Sibeck [1993] for the solar wind dynamic pressure of 0.5 nPa and IMF Bz = 0 **observed by THEMIS B and C (see below),** while the location of the Fairfield [1971] bow shock was scaled to place THEMIS B and C in the solar wind during this interval.

From 2313 to 2323 UT on October 15, 2008 all three THEMIS A, D and E spacecraft in the magnetosphere observed a long-duration (~10 min) transient event with magnetic field perturbations characteristic of FTEs. Figure 2 presents the magnetic field and plasma moments in GSM coordinates from 2300 UT to 2340 UT observed by THEMIS A, which was closest to the magnetopause and saw stronger magnetic field and plasma signatures. The transient event at 2319 UT was marked by bipolar (-,+) and (+,-) 5 nT signatures in the Bx and By components, respectively, a positive monopolar variation in the Bz component, and a ~ 13 nT enhancement in the total magnetic field strength. The event is superimposed upon an abrupt increase in the total magnetic field strength at THEMIS A from a minimum value of 37 nT before the event to a maximum value of 42 nT after the event. THEMIS D and E observed similar ~13 nT enhancements in the total magnetic field strength (not shown). However, THEMIS A observed a sharper increase in the magnetic field strength and greater perturbations in the Bx and By components, presumably because it was closer to the magnetopause. The transients might be FTEs or waves on the boundary. In either case, they correspond to only slight indentations on the magnetopause. In the ~45 nT magnetic field observed by

THEMIS A, a 5 nT perturbation in the direction normal to the nominal magnetopause corresponds to a ~6° indentation in the magnetopause surface.

The plasma observations also show transient features typical of magnetospheric FTEs: an increase in density, decrease in temperature, northward (+Vz) and sunward (+Vx) flows, a bipolar (+,-) variation in the Vy component, and a ~ 120 km/sec increase in the total velocity. As described by Korotova et al. [2009], the passage of FTEs displaces the ambient media. Signatures to be observed by a spacecraft within the magnetosphere include inward/outward flow velocities in the direction normal to the nominal magnetopause and flows opposite the direction of event motion (here the Vx and Vz signatures). The northward and sunward flows observed in the magnetosphere outside this event indicate that the event itself was moving southward and antisunward along the magnetopause.

As in the previous study of Korotova et al. [2011], we interpret the event in terms of a transient magnetospheric compression and not a burst of reconnection. There are two reasons for this. First, the event is long (~10 min) and was observed deep within the magnetosphere. Such events have previously been attributed to pressure pulses [e.g., Korotova et al., 2011]. Second, the southward and antisunward motion of the event inferred from perturbations in the flow velocities is inconsistent with the postulated location of THEMIS A northward and dawnward of a tilted subsolar reconnection line for the observed duskward and southward IMF orientation [Korotova et al., 2009].

Figure 3 presents GOES 11 and GOES 12 magnetic field observations at early and late post-noon local times, respectively. They show that the magnetospheric compression at the time of the transient event was widespread, consistent with the suggested

interpretation of the event [e.g., Korotova, et al., 1997, 2004]. GOES 11 (~1420 LT) observed bipolar magnetic field signatures in the Bx component indicating an indentation while GOES 12 (~1820 LT) does not.

Table 1. Arrival times of peak magnetospheric compressions in the transient event observed by THEMIS A, D, E and GOES 11/12 and the discontinuity observed by THEMIS B and C

Spacecraft	Observed Peak Time (UT)	Fit Peak Time (UT)
THEMIS B	2319:48	
THEMIS C	2315:33	
GOES-11	2318:03	2318:06
THEMIS E	N.A.	2318:39
GOES-12	2319:34	2319:21
THEMIS D	2319:15	2319:24
THEMIS A	2319:36	2319:40

The high time resolution data **shown in Figure 4** lets us time the motion of the transient event through the magnetosphere. **Only the perturbations are shown, a (different) constant value has been removed from each of the traces. We employ two methods**. First, we compare the times of the magnetospheric magnetic field strength maxima observed by GOES-11/12 and THEMIS A and D with the times at the centers of the magnetosheath intervals observed by THEMIS B and C. This method does not work for THEMIS E because this spacecraft observed a more complicated signature with at least two peaks in the total magnetic field strength. The results, shown in the second column of Table 1, indicate event motion from GOES-11 dawnward towards the other

spacecraft and duskward to GOES-12. **Second, to estimate the errors involved in this method, we also fit higher order polynomials to 5-7 min long intervals encompassing the magnetospheric events and compared the peak values in the fits to the times at the centers of the magnetosheath intervals observed by THEMIS B and C. The results, shown in the third column of Table 2, confirm the sense of propagation and differ by 3-13s from those obtained by the first method. For future reference, note that the magnetic field strength begins to increase at 2301 UT at GOES-11 and near 2303 UT at GOES-12.**

In search of solar wind triggers for the transient magnetospheric compression we inspected ACE, Wind and THEMIS B and C observations for corresponding signatures. ACE was located far upstream at ~ 244 R_E during the period of interest and the lag time for the propagation of disturbances to the Earth was about one hour. Figure 5 presents ACE magnetic field and velocity observations from 2200 UT to 2240 UT. ACE observed a discontinuity at ~ 2218 UT, when it was located at GSM (X, Y, Z) = (242.0, -25.6, -18.6) R_E. Although the discontinuity was more complicated than a simple rotational or tangential discontinuity, we calculated its normal as the cross-product **n= (B1xB2)/(|B1xB2|),** where **B1** and **B2** are the mean magnetic fields before and after the discontinuity. The result of the calculation is presented in Table 2 and indicates that the normal pointed dawnward, southward, and antisunward. Solar wind discontinuities with this orientation should first encounter the post-noon bow shock and then sweep southward and both dawnward and duskward, consistent with the aforementioned observations. Wind lies far (~90 R_E) off the Sun-Earth line during the period of interest.

213 Because its observations do not indicate a single pronounced discontinuity and differ
214 strikingly from those at ACE, we use ACE as the appropriate distant upstream monitor.
215 THEMIS B and C were located closer to Earth and provide us with better
216 opportunities to study upstream conditions. Figures 6 and 7 present their observations of
217 the ion flux spectra, magnetic field, and plasma in the vicinity of the bow shock from
218 2300 UT to 2340 UT. The interval can be divided into three very different parts. F**rom**
219 **2300 to 2314:42 UT at THEMIS C and from 2300 to 2318:12 UT at THEMIS B), the**
220 **spacecraft were in the quasi-parallel foreshock as indicated by $\Theta_{Bn} < 45°$, where Θ_{Bn}**
221 **is the angle between the interplanetary magnetic field and the normal to the local**
222 **portion of the scaled Fairfield bow shock**. The foreshock intervals were characterized
223 by disturbed and slightly negative Bx and Bz components, a positive By component and a
224 total magnetic field strength of ~5 nT. This spiral IMF orientation connected the
225 spacecraft to the pre-noon bow shock. Plasma parameters provide further evidence for
226 increased wave activity during the foreshock. The plasma flow was predominantly
227 antisunward with a velocity of ~320-330 km/sec, density and temperatures oscillated near
228 2 cm^{-3} and 100 eV, respectively. The dynamic pressure was ~0.3-0.4 nPa. **IMF Bz was**
229 **near zero.** As expected on the basis of past work, the velocity within the foreshock
230 observed by THEMIS B and C (Vx and Vtot) was slower than that observed by ACE in
231 the pristine solar wind. Finally, the ion flux energy spectra show the presence of
232 superthermal ions with energies of ~10 keV, a good indicator of the foreshock [Fairfield
233 at el., 1990].
234 The bow shock moved outward during the second interval, from ~ **2314:42** UT at
235 THEMIS C and ~2318:12 UT at THEMIS B for 2-3 min. These are magnetosheath

intervals because the density and temperature increased to 8-9 nT and 150-250 eV, respectively, the total velocity decreased to 150-180 km/sec, the velocities were deflected dawnward, and the ion flux energy spectra broadened indicating the presence of 0.01-1 keV ions. Although there are sharp increases in density and magnetic field strength on one or both sides of these intervals, these are not the signatures of hot flow anomalies, which are identifiable on the basis of density decreases, sharp flow deflections, and large temperature increases. **Because THEMIS C was at least 0.5 R_E further from the bow shock along its local normal than THEMIS B was from the bow shock along its local normal, the amplitude of the bow shock motion was at least 0.5 R_E.**

The third interval occurred after the bow shock moved back Earthward past THEMIS C at 2316:24 UT and THEMIS B at 2321:24 UT. The Bx components of the magnetic field became positive, resulting in orthospiral IMF orientations that **did not connect the THEMIS spacecraft to the bow shock. Upon exiting the magnetosheath, the spacecraft were initially in a transitional region between the quasi-parallel and quasi-perpendicular foreshock with $\Theta_{Bn} \sim 45°$. After 4-5 min, Θ_{Bn} increased greatly, indicating that the magnetic field pointed nearly perpendicular to the nominal normal to the bow shock.** As a result, wave activity in the magnetic field and plasma parameters stopped and these parameters became steady. The total magnetic field strength and temperatures decreased to 3 nT and 30 eV, respectively, but the density increased up to 3.2 cm^{-3}. The solar wind dynamic pressure increased to 0.5-0.6 nPa. **IMF Bz was near zero.** The ~10 keV ions disappeared from the energy spectra. There was not much change in the THEMIS plasma flow: the Vz component decreased from ~ -25 to ~ 0 km/s, i.e., the flow became less southward. Contrary to THEMIS, ACE did not

observe any change in the Vz component while the Vy component decreased from ~17-20 nT to -5-0 nT after the discontinuity. Discrepancies in the ACE and THEMIS Vy and Vz components could be due to spatial variations in the solar wind.

As indicated in Table 1, THEMIS C saw the rotation in the IMF and outward motion of the bow shock before B. It took ~ 4:15 min for the IMF discontinuity to propagate from C (2315:33 UT) to B (2319:48 UT), indicating an IMF discontinuity with a normal very inclined to the Sun-Earth line that is moving slowly dawnward. To determine the orientation of the interplanetary discontinuity from the THEMIS B and C observations, we assumed that it was a tangential discontinuity and calculated its normal as a cross-product. Table 2 presents the results for the normals to the discontinuity observed by THEMIS B and C. As in the case of the ACE observations, they indicate that the normal to the discontinuity pointed dawnward, southward, and antisunward. Differences in the precise orientations of the discontinuities at ACE, THEMIS B, and THEMIS C result from errors, spatial variations in the interplanetary discontinuity, and perturbations associated with disturbed magnetic field directions in the foreshock. The arrow in the bottom left corner of Figure 1 illustrates the normal to the tangential discontinuity calculated from THEMIS B observations. Using the positions of THEMIS B and C, the observed 330 km s^{-1} solar wind velocity, and the normal for the discontinuity calculated from the THEMIS B observations, we estimate a lag time of ~7 min from THEMIS C to B, somewhat longer than that observed, confirming that although the sense of the normal to the discontinuity is correct, its precise orientation is not very well determined.

We should also compare the time when the discontinuity passes THEMIS C to the time when its effects are felt in the magnetosphere. THEMIS C encounters the magnetosheath during an interval centered on 2315:33 UT. Using the normal to the interplanetary magnetic field discontinuity computed from the THEMIS B observations and the observed solar wind velocity, we find that the interplanetary magnetic field discontinuity should have encountered the bow shock at a position directly upstream from the GOES-11 spacecraft at GSM (x, y, z) = (14, 4, 0) R_E, some 17 min before it reached THEMIS C, i. e. at 2258 UT. Past studies indicate that IMF features require 4-8 min to cross the magnetosheath [Freeman and Southwood, 1988; Etemadi et al., 1988]. The resulting arrival times of 2302 to 2306 UT are slightly later than the time when the magnetospheric magnetic field strength begins to increase at GOES-11, about 2301 UT according to Figure 4.

Normals to the bow shock crossings observed by THEMIS B and C oscillate in the manner expected for an antisunward and dawnward propagating wave on the bow shock. We used the coplanarity theorem for estimating shock normals [Lepping and Argentiero, 1971] to determine the orientation of the bow shock at its crossings by THEMIS B and C, **n=± (B1xB2) X (B2-B1)/|(B1xB2) X (B2-B1)|,** where B1 and B2 are the mean magnetic fields before and after the bow shock crossings. Table 2 presents results from these normal calculations. Figure 1 shows the normals (n1, n2, n3, n4) to the modified bow shock shape as the "bulge" passes THEMIS C and B. **The bulges are shown at two times. First (solid curve), when only the outward bulge is present on the bow shock. Second (dashed curve) when an outward bulge is present on the dawn bow shock and an inward bulge (grey curve) on the post-noon magnetopause.**

305 The normals are deflected from directions expected for the nominal bow shock
306 and oscillate in the manner expected for an antisunward and southward moving wave on
307 the bow shock boundary, as expected for the derived orientation of the driving
308 interplanetary discontinuity. The similarity of the normals observed by THEMIS B and
309 C (see Table 2) suggest that the shape of the bulge did not change much as it propagated
310 dawnward from THEMIS C to THEMIS B.
311 Knowing that the bow shock moved outward from ~**2314:42 to** 23:16:24 UT at
312 THEMIS C and from ~2318:12 to 2321:24 UT at THEMIS B we determined that the
313 outward bulge on the bow shock moved dawnward with a velocity of ~251 km/sec.
314 Given the durations of the event at each location, this bulge had a dimension of 4.8 R_E
315 in the vicinity of THEMIS C and 7.55 R_E in the vicinity of THEMIS B. **Since THEMIS**
316 **C was located ~0.5 R_E further from the average position of the bow shock than**
317 **THEMIS B, we suppose that THEMIS C observed the crest of the bulge while**
318 **THEMIS B observed its full width.**
319 Summarizing the results of this section, the sequence of events observed by THEMIS B
320 and C suggests an explanation in which the bow shock briefly moved outward, perhaps
321 by a transient decrease in the solar wind dynamic pressure applied to the magnetosphere.
322 By contrast, the sequence of event observed by all the spacecraft in the magnetosphere
323 suggests an explanation in which the magnetosphere was briefly compressed, perhaps by
324 a transient increase in the solar wind dynamic pressure. The observations could be
325 reconciled if the IMF discontinuity caused a transient outward motion of the bow shock
326 in addition to launching a transient pressure increase into the magnetosheath. To test this
327 hypothesis, we must examine the predictions of a global hybrid code model.

Table 2. Solar Wind Discontinuity and Bow Shock Normals

Spacecraft	Representative Times	Bow Shock nx	ny	nz	Discontinuity nx	ny	nz
ACE	2216:13 - 2219:25				-0.41	-0.36	-0.89
THEMIS C	2313:55 - 2316:32				-0.23	-0.73	-0.64
THEMIS B	2317:38 - 2322:05				**-0.37**	**-0.59**	**-0.71**
THEMIS C	2314:28 - 2314:58	0.40	-0.72	-0.56 (n1)			
THEMIS C	2316:05 - 2316:38	-0.89	-0.31	-0.34 (n2)			
THEMIS B	2317:59 - 2318:32	0.48	-0.86	-0.38 (n3)			
THEMIS B	2321:15 - 2321:45	-0.88	-0.47	0.03 (n4)			

4. Description of global hybrid code model.

We examine output from a global hybrid model similar to that presented by Omidi and Sibeck [2007] in which ions are treated kinetically via particle-in-cell methods and electrons form a massless fluid. The simulation plane corresponds to the noon-midnight meridion plane with Y pointing northward (see Figure 8). Solar wind plasma enters the simulation domain from the left boundary and leaves through the three remaining boundaries. Although the magnetosphere is 7 times smaller than that of the Earth, the model still captures the relevant physics. The simulation retains all three components of the electromagnetic fields and plasma flows. The solar wind Alfvén Mach number is set to 12, ion and electron betas are set to 0.3. Cell sizes in the

353 simulation are 1 c/ω_{pi} where c is the speed of light and ω_{pi} is the proton plasma frequency,
354 and the resistive scale length is 0.3 c/ω_{pi}. The simulation box extends to 2000 c/ω_{pi} in X
355 and Y directions respectively with the Earth's dipole centered at X = 1500 and Y = 1250.
356 Prior to the arrival of the tangential discontinuity, the IMF lies in the X-Y (meridional)
357 plane, whereas it rotates at the discontinuity to develop a duskward Z component. There
358 is no change in the magnetic field strength, density, velocity, or temperature across the
359 discontinuity.

360 Figure 8 shows a color intensity plot of the predicted density normalized to the
361 solar wind density in a region centered on the southern foreshock and the bow shock. We
362 wish to call attention to two features: (1) an outward motion of the bow shock following
363 the passage of the tangential discontinuity and (2) a front marked by a transient increase
364 in the density (pressure) launched into the magnetosheath.

365 Concerning the first topic, we note that a highly turbulent foreshock lies
366 upstream from the quasi-parallel bow shock at locations antisunward (to the right) of the
367 tangential discontinuity. By contrast, the solar wind is in a pristine condition upstream
368 from the quasi-perpendicular bow shock at locations sunward (to the left) of the
369 tangential discontinuity. As indicated by the density contours in Figure 8, the passage of
370 the discontinuity causes the bow shock to move outward from a position nearer Earth in
371 the quasi-parallel configuration to one further from Earth in the quasi-perpendicular
372 configuration. These results are consistent with results from the simulation reported by
373 Thomas and Winske [1990], a observations from Venus reported by Zhang et al. [1991],
374 **and observations of the terrestrial bow shock reported in Figure 5 of Verigin et al.**
375 **2001].** Because the bow shock lies along the locus of points where the components of the

376 solar wind velocity and magnetosheath fast mode speed normal to the bow shock balance,
377 and fast mode speeds are greater perpendicular than parallel to magnetosheath magnetic
378 fields, theory predicts outward bow shock motion for a transition from quasi-parallel to
379 intermediate or quasi-perpendicular shocks.

380 The actual tangential discontinuity on October 15, 2008 was accompanied by an
381 increase in the solar wind density and therefore dynamic pressure, as indicated by the
382 jumps in density from times before the magnetosheath encounters to times after the
383 magnetosheath encounters in Figures 6 and 7. This increase in the solar wind dynamic
384 pressure should push the bow shock (and magnetopause) inward, not outward. The
385 actual motion of the bow shock must therefore be the sum of the outward motion
386 associated with the rotation in the IMF direction and inward motion associated with the
387 step function increase in the solar wind dynamic pressure. The outward motion of the
388 bow shock can therefore be transient.

389 To simulate the sequence of events that would be observed by a spacecraft
390 initially just upstream from the quasi-parallel bow shock during the passage of the
391 tangential discontinuity, we take a cut of the plasma and magnetic field observations
392 along the line labeled "L" in Figure 8 that grazes the bow shock. Figure 9 shows that the
393 spacecraft first observes the turbulent quasi-parallel foreshock, briefly enters the
394 magnetosheath, and then reenters the solar wind upstream from the quasi-perpendicular
395 bow shock. This is very similar to the scenarios seen by THEMIS B and C, as shown in
396 Figures 6 and 7.

397 Concerning the second topic, we note that the simulation indicates the
398 transmission of a transient density increase into the magnetosheath. To simulate the

399 sequence of events that would be observed by a spacecraft initially in the magnetosheath,
400 we take a cut of the plasma and magnetic field observations across this increase, i.e.
401 along the line labeled "L1" in Figure 8. Figure 10 shows that the spacecraft observes a
402 transient increase in the density and dynamic pressure, but no significant change in the
403 total velocity, temperature, or magnetic field strength as the density front passes by. This
404 transient increase in density must be added to the step function increase in the solar wind
405 density observed on October 15, 2008, resulting in a transient compression of the
406 magnetosphere superimposed upon a step function increase in magnetospheric magnetic
407 field strengths. Inspection of Figures 2 and 3 shows that this is precisely the case for the
408 THEMIS A and GOES 11 magnetospheric magnetic field strength observations.
409
410 **5. Conclusions**

411 We presented a multipoint THEMIS case study of a transient event observed
412 inside the pre-noon magnetopause at 2319 UT on October 15, 2008. Multipoint
413 observations indicate a global compression of the magnetosphere corresponding to a
414 transient outward bow shock motion. We used results from a global hybrid code model
415 for the interaction of an IMF tangential discontinuity with the bow shock to reconcile the
416 observations. The arrival of a discontinuity that transforms the bow shock from quasi-
417 parallel to quasi-perpendicular launches a narrow density front into the magnetosheath
418 that briefly compresses the magnetosphere when it strikes the magnetopause. The same
419 discontinuity initiates outward bow shock motion and contributes to an additional
420 compression of the magnetospheric magnetic field.
421
422 **Acknowledgements.** Work at GSFC was supported by the THEMIS project, while

423 work by G. I. K. at the University of Maryland was supported by a grant from
424 NASA/GSFC NNX09AV52G.
425

426 **References**

427 Andreeova, K., T. I. Pulkkinen, L. Juusola, M. Palmroth, and O. Santolik, Propagation of
428 a shock-related disturbance in the Earth's magnetosphere, J. Geophys. Res., 116,
429 doi:10.1029/2010JA015908, 2011.
430 Auster, U., K.-H. Glassmeier, S. P. Rounds, et al., The THEMIS Fluxgate Magnetometer,
431 Space Sci. Rev., 141, 235-264, doi:10.1007/s11214-008-9365-9, 2008.
432 Cable, S. and Y. Lin, Three-dimensional MHD simulations of interplanetary rotational
433 discontinuities impacting the Earth's bow shock and magnetosheath, J. Geophys.
434 Res., 103, 29551-29568, 1998.
435 Etemadi, A., S. W. H. Cowley, M. Lockwood, B. J. I. Bromage, and D. M. Willis, The
436 dependence of high-latitude dayside ionospheric flows on the north-south
437 component of the IMF- A high time resolution correlation analysis using EISAT
438 'Polar' and AMPTE UKS and IRM data, Planet. Space Sci., 36, 471-498, 1988.
439 Fairfield, D. H., Average and unusual locations for the earth's magnetopause and bow
440 shock, J. Geophys. Res., 76, 6700 – 6716, 1971.
441 Fairfield, D. H., W. Baumjohann, G. Paschman, H. Luhr, and D. G. Sibeck, Upstream
442 pressure variations associated with the bow shock and their effects on the
443 magnetosphere, J. Geophys. Res., 95, 3773 – 3786, 1990.
444 Freeman, M. P. and D. J. Southwood, The correlation of variations in the IMF with
445 magnetosheath field variations, Adv. Space Res., 8, 217-220, 1988.

446 Kaufmann, R. L., Shock observations with the Explorer 12 magnetometer, J. Geophys.
447 Res., 72, 2323-2342, 1967.
448 Keika, K., R. Nakamura, W. Baumjohann, V. Angelopoulos, K. Kabin, K.-H. Glaßmeier,
449 D. G. Sibeck, W. Magnes, H. U. Auster, K. H. Fornacon, J. P. McFadden, C. W.
450 Carlson, E. A. Lucek, C. M. Carr, I. Dandouras, and R. Rankin, Deformation and
451 evoluition of solar wind discontinuities through their interactions with the Earth's
452 bow shock, J. Geophys. Res., 114, doi:10.1029/2008JA013481, 2009.
453 Korotova, G. I., D. G. Sibeck, T. J. Rosenberg, C. T. Russell, and E.Friis-Christensen,
454 High-latitude ionospheric transient events in a global context, J. Geophys. Res.,
455 102, 17499- 17508, 1997.
456 Korotova G. I., D. G. Sibeck, H. Singer, T. J. Rosenberg, Tracking transient events
457 through geosynchronous orbit and in the high-latitude ionosphere, J. Geophys.
458 Res., 107, doi:10.1029/2002JA009477, 2002.
459 Korotova, G. I., Sibeck, D. G., Singer, H. J., Rosenberg, T. J., Multipoint observations of
460 transient event motion through the ionosphere and magnetosphere, in NATO
461 Science Series Book: Multiscale processes in the Earth's magnetosphere: from
462 Interball to Cluster, edited by J.-A. Sauvaud, and Z. Nemecek, Kluwer Academic
463 Publishers, Dordrecht/Boston/London, 205- 216, 2004.
464 Korotova, G. I., D. G. Sibeck, and T. Rosenberg, Geotail observations of FTE velocities,
465 Ann. Geophys., 27, 83-92, 2009.
466 Korotova, G. I., and D. G. Sibeck, A. Weatherwax, V. Angelopoulos, V. Styazhkin,
467 THEMIS observations of a transient event at the magnetopause, J. Geophys.
468 Res., 2011.

469 Koval, A., J. Safrankova, Z. Nemecek, L. Prech, A. A. Samsonov, and J. D. Richardson,
470 Deformation of interplanetary shock fronts in the magnetosheath, Geophys. Res.
471 Lett., 32, doi:10.1029/2005GL023009, 2005.
472 Koval, A., J. Safrankova, Z. Nemecek, A. A. Samsonov, L. Prech, J. D. Richardson, and
473 M. Hayosh, Interplanetary shock in the magnetosheath: Comparison of
474 experimental data with MHD modeling, Geophys. Res. Lett., 33,
475 doi:10.1029/2006GL025707, 2006.
476 Lemaire, J., Impulsive penetration of filamentary plasma elements into the
477 magnetospheres on the Earth and Jupiter, Planet. Space Sci., 25, 887, 1977.
478 Lepping, R. P., and P. D. Argentiero, Single spacecraft method of estimating shock
479 normals, J. Geophys. Res., 76, 4349-4359, 1971.
480 Merka, J., A. Szabo, J. A. Slavin, and M. Peredo, Three-dimensional
481 position and shape of the bow shock and their variation with upstream
482 Mach numbers and interplanetary magnetic field orientation, J.
483 Geophys. Res., 110, 10.10290/2004JA010944, 2005.
484 McFadden, J. P., C.W. Carlson, D. Larson, et al., The THEMIS ESA Plasma Instrument
485 and In-flight Calibration, Space Sci. Rev., 141, 277, doi:10.1007/s11214-008-
486 9440-2, 2008.
487 Nemecek, Z., J. Safrankova, A. Koval, J. Merka, and L. Prech, MHD analysis of
488 propagation of an interplanetary shock across magnetospheric boundaries, J.
489 Atmo. Solar-Terr. Phys, 73, 20-29, 2011.
490 Omidi, N. and D. G. Sibeck, Flux transfer events in the cusp, Geophys. Res. Lett., 34,
491 L04106, doi:10.1029/2006GL028698, 2007.

492 Omidi, N., D. G. Sibeck, and X. Blanco-Cano, Foreshock compressional
493 boundary, J. Geophys. Res., 114, 10.1029/2008JA013950, 2009.
494 Paschmann, G., G. Haerendel, N. Sckopke, E. Moebius, and H. Luehr, Three-dimensional
495 plasma structures with anomalous flow directions near the Earth's bow shock, J.
496 Geophys. Res., 93, 11279-11294, 1988.
497 Roelof, E. C. and D. G. Sibeck, Magnetopause shape as a bivariant function of
498 interplanetary magnetic field Bz and solar wind dynamic pressure, J. Geophys.
499 Res., 98, 21421-21450, 1993.
500 Russell C. T., and R. C. Elphic, Initial ISEE magnetometer results: Magnetopause
501 observations, Space Sci. Rev., 22, 681-715, 1978.
502 Safrankova, J., Z. Nemecek, L. Prech, A. A. Samsonov, and A. Koval, Interaction of
503 interplanetary shocks with the bow shock, Planet. Space Sci., 55, 2324-2329,
504 2007.
505 Samsonov, A. A., D. G. Sibeck, and J. Imber, MHD simulation for the interaction of an
506 interplanetary shock with the Earth's magnetosphere, J. Geophys. Res., 112,
507 10.1029/2007JA012627, 2007.
508 Shue, J.-H., J. K. Chao, H. C. Fu, C. T. Russell, P. Song, K. K. Khurana, and H. J.
509 Singer, A new functional form to study the solar wind control of the
510 magnetopause size and shape, J. Geophys. Res., 102, 9497-9512, 1997.
511 Sibeck, D. G., W. Baumjohann, and R. E. Lopez, Solar wind dynamic pressure variations
512 and transient magnetospheric signatures, Geophys. Res. Lett., 16, 13-16, 1989.
513 Sibeck, D. G., N. L. Borodkova, S. J. Schwartz, C. J. Owen, R. Kessel, S. Kokubun, R. P.
514 Lepping, R. Lin, K. Liou, H. Luehr, R. W. McEntire, C.-I. Meng, T. Mukai, Z.

515 Nemecek, G. Parks, T. D. Phan, S. A. Romanov, J. Safrankova, J.-A. Sauvaud, H.
516 J. Singer, S. I. Solovjev, A. Szabo, K. Takahashi, D. J. Williams, K. Yumoto, and
517 G. N. Zastenker, J. Geophys. Res., 104, 4577-4594, 1999.
518 Singer, H. J., L. Matheson, G. Gribb, A. Newman, and S. D. Bouwer, Monitoring space
519 weather with the GOES magnetometers, SPIE-Proceedings GOES-8 and beyond,
520 ed. E. R. Washwell, 2812, 299-308, 1996.
521 Southwood, D. J., Magnetopause Kelvin-Helmholtz instability, in Magnetospheric
522 Boundary Layers, edited by B. Battrick, Eur. Space Agency Spec. Publ., SP-148,
523 357-364, 1979.
524 Thomas, V. A. and D. Winske, Two-dimensional hybrid simulation of a curved bow
525 shock, Geophys. Res, Lett., 1-7, 1247, 1990.
526 Verigin, M. I., G. A. Kotova, J. Slavin, A. Szabo, M. Kessel, J. Safrankova, Z. Nemecek,
527 T. I. Gombosi, K. Kabin, F. Shugaev, and A. Kalinchenko, Analysis of the 3-d
528 shape of the terrestrial bow shock by Interball/Magion 4 observations, Adv. Space
529 Res., 28, 857-862, 2001.
530 Voelk, H. J. and R. D. Auer, Motions of the bow shock induced by interplanetary
531 disturbances, J. Geophys. Res., 79, 40-48, 1974.
532 Volwerk, M., J. Berhem, Y. V. Bogdanova, O. D. Constantinescu, M. W. Dunlop, J. P.
533 Eastwood, P. Escoubet, A. N. Fazakerley, H. Frey, H. Hasegawa, B. Lavraud, E.
534 V. Panov, C. Shen, J. K. Shi, M. G. G. T. Taylor, J. Wang, J. A. Wild, Q. H.
535 Zhang, O. Amm, and J. M. Weygand, Interplanetary magnetic field rotations
536 followed from L1 to the ground: the response of the Earth's magnetosphere as

seen by multi-spacecraft and ground-based observations, Ann. Geophys., 29, 1549-1569, 2011.

Wu, B.-H., M. E. Mandt, L. C. Lee, and J. K. Chao, Magnetospheric response to solar wind dynamic pressure variations: Interaction of interplanetary tangential discontinuities with the bow shock, J. Geophys. Res., 98, 21297-21311, 1993.

Zhang, H., Q.-G. Zong, D. G. Sibeck, T. A. Fritz, J. P. McFadden, K.-H. Glaßmeier, and D. Larson, Dynamic motion of the bow shock and the magnetopause observed by THEMIS spacecraft, J. Geophys. Res., 114, doi:10.1029/2008JA013488, 2009.

Zhang, T.L., K. Schwingenschuh, C. T. Russell, and J. G. Luhmann, Asymmetries in the location of the Venus and Mars bow shock [Preview], Geophys. Res. Lett., 18, 2, doi:10.1029/90GL02723, 1991.

Figure Captions

Fig.1. Locations of THEMIS A, B, C, D, E and GOES 11 and 12 in the GSM X-Y plane from 2230 UT to 2400 UT on October 15, 2008. **The bulges are shown at two times. First (solid curve), when only the outward bulge is present on the bow shock. Second (dashed curve) when an outward bulge is present on the dawn bow shock and an inward bulge (grey curve) on the post-noon magnetopause.** Normals (n1, n2, n3, n4) to the modified bow shock (BS) shape are shown as the "bulge" passes THEMIS C and B. The curve labeled MP shows the corresponding inferred inward deformations of the magnetopause. The arrow in the bottom left corner of the figure illustrates the normal to the tangential discontinuity observed by THEMIS B.

559 Fig.2. THEMIS A plasma and magnetic field observations from 2300 UT to 2340 UT on
560 October 15, 2008. From top to bottom, the panels show the Bx, By, Bz components of
561 magnetic field in GSM coordinates and total magnetic field strength, the ion density, the
562 velocities in GSM coordinates, the ion temperatures perpendicular and parallel to
563 magnetic field. **Dashed lines bound the transient event.**
564
565 Fig. 3. GOES-11 and -12 magnetic field observations in GSM coordinates from 2300 UT
566 to 2340 UT on October 15, 2008. Arrows show a compression of the magnetosphere.
567
568 **Fig. 4. Variations in the total magnetic field strength observed by GOES-11 and -**
569 **12, THEMIS A and D from 2300 to 2330 UT on October 15, 2008. A constant value**
570 **has been subtracted from each trace so that they can be graphed on the same scale.**
571
572 Fig. 5 ACE observations of the magnetic field and velocity in GSM coordinates from
573 2200 UT to 2240 UT on October 15, 2008. The arrow indicates a discontinuity.
574
575 Fig. 6. THEMIS C observations of ion energy spectra, plasma and magnetic field from
576 2300 UT to 2340 UT on October 15, 2008. From top to bottom, the panels show the flux
577 spectrogram for ions in the range of energies from 2 eV to 25 keV (ESA), **Θ_{Bn}, the angle**
578 **between the magnetic field and the local bow shock normal, dynamic pressure, Bx,**
579 **By, Bz components of magnetic field in GSM coordinates and total magnetic field,**
580 **the ion density, the velocities in GSM coordinates, the ion temperatures**
581 **perpendicular and parallel to magnetic field. The spacecraft began the interval in**

582 **the quasi-parallel foreshock (Θ_{Bn} < 45°). Two vertical dashed lines bound a brief**
583 **period in the magnetosheath. Upon exiting the magnetosheath, the spacecraft was**
584 **in a transitional region between the quasi-parallel and quasi-perpendicular**
585 **foreshock (Θ_{Bn} ~ 45°). The third vertical dashed line marks the transition to the**
586 **quasi-perpendicular bow shock (Θ_{Bn} > 45°).**
587
588 Fig. 7. The same as for Fig.6 except for THEMIS B observations.
589
590 Fig. 8. Color intensity plot of density in the run for a portion of the simulation box (noon-
591 midnight meridian plane) containing the dayside and post-noon bow shock. The density
592 is normalized to the solar wind density, X points antisunward and Y points northward.
593
594 Fig.9. Snapshots of ion Vx and Vy velocities, magnetic field strength, and density along
595 the cut labeled "L" in Figure 8. Velocities are normalized to the Alfvén speed in the solar
596 wind while the magnetic field and density are normalized to their corresponding values in
597 the solar wind.
598
599 Fig.10. Snapshots of magnetic field strength, temperature, magnitude of the ion velocity,
600 density and dynamic pressure along the cut labeled "L1" in Figure 8. Velocity is
601 normalized to the Alfvén speed in the solar wind while the magnetic field and density are
602 normalized to their corresponding values in the solar wind.
603
604

605

606

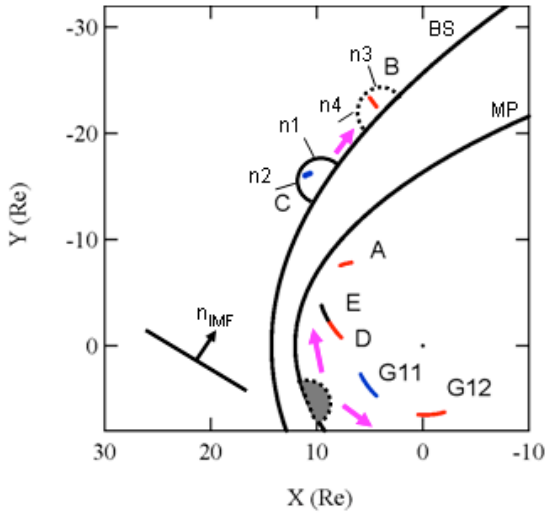

607

608

609 Fig.1. Locations of THEMIS A, B, C, D, E and GOES 11 and 12 in the GSM X-Y plane
610 from 2230 UT to 2400 UT on October 15, 2008. **The bulges are shown at two times.**
611 **First (solid curve), when only the outward bulge is present on the bow shock.**
612 **Second (dashed curve) when an outward bulge is present on the dawn bow shock**
613 **and an inward bulge (grey curve) on the post-noon magnetopause.** Normals (n1, n2,
614 n3, n4) to the modified bow shock (BS) shape are shown as the "bulge" passes THEMIS
615 C and B. The curve labeled MP shows the corresponding inferred inward deformations of
616 the magnetopause. The arrow in the bottom left corner of the figure illustrates the normal
617 to the tangential discontinuity observed by THEMIS B.

618

619

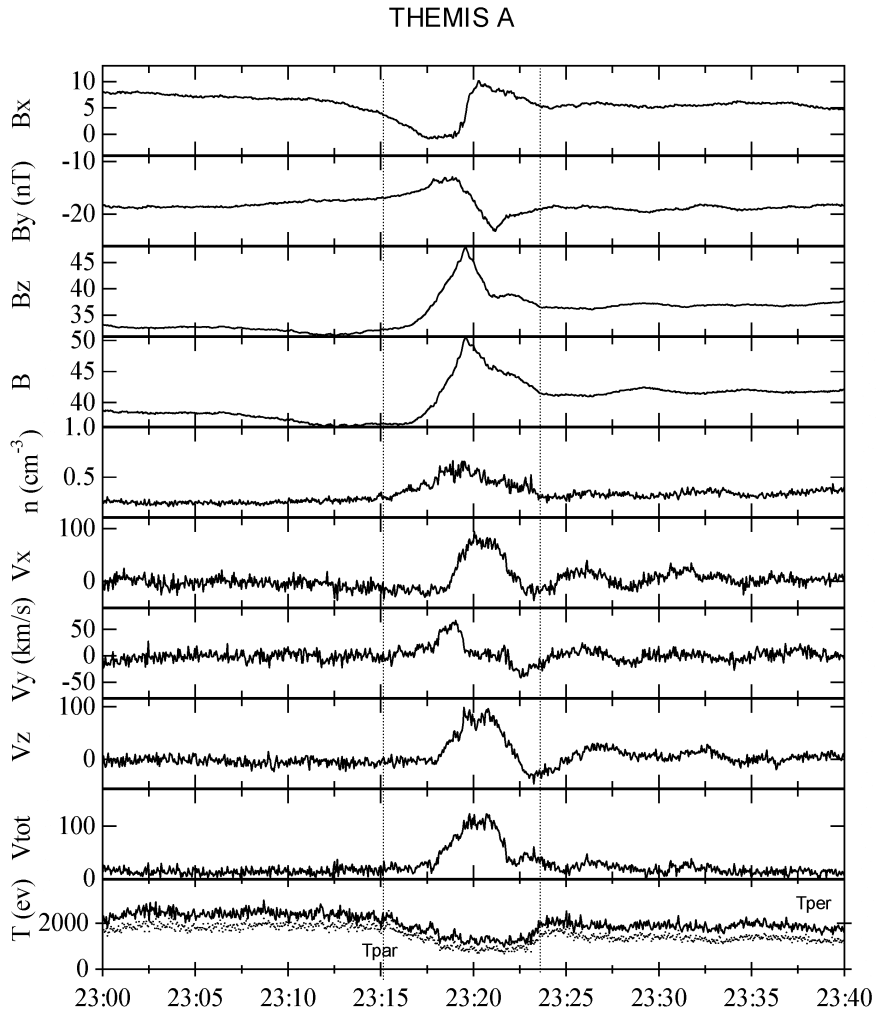

Fig.2. THEMIS A plasma and magnetic field observations from 2300 UT to 2340 UT on October 15, 2008. From top to bottom, the panels show the Bx, By, Bz components of magnetic field in GSM coordinates and total magnetic field strength, the ion density, the velocities in GSM coordinates, the ion temperatures perpendicular and parallel to magnetic field. **Dashed lines bound the transient event.**

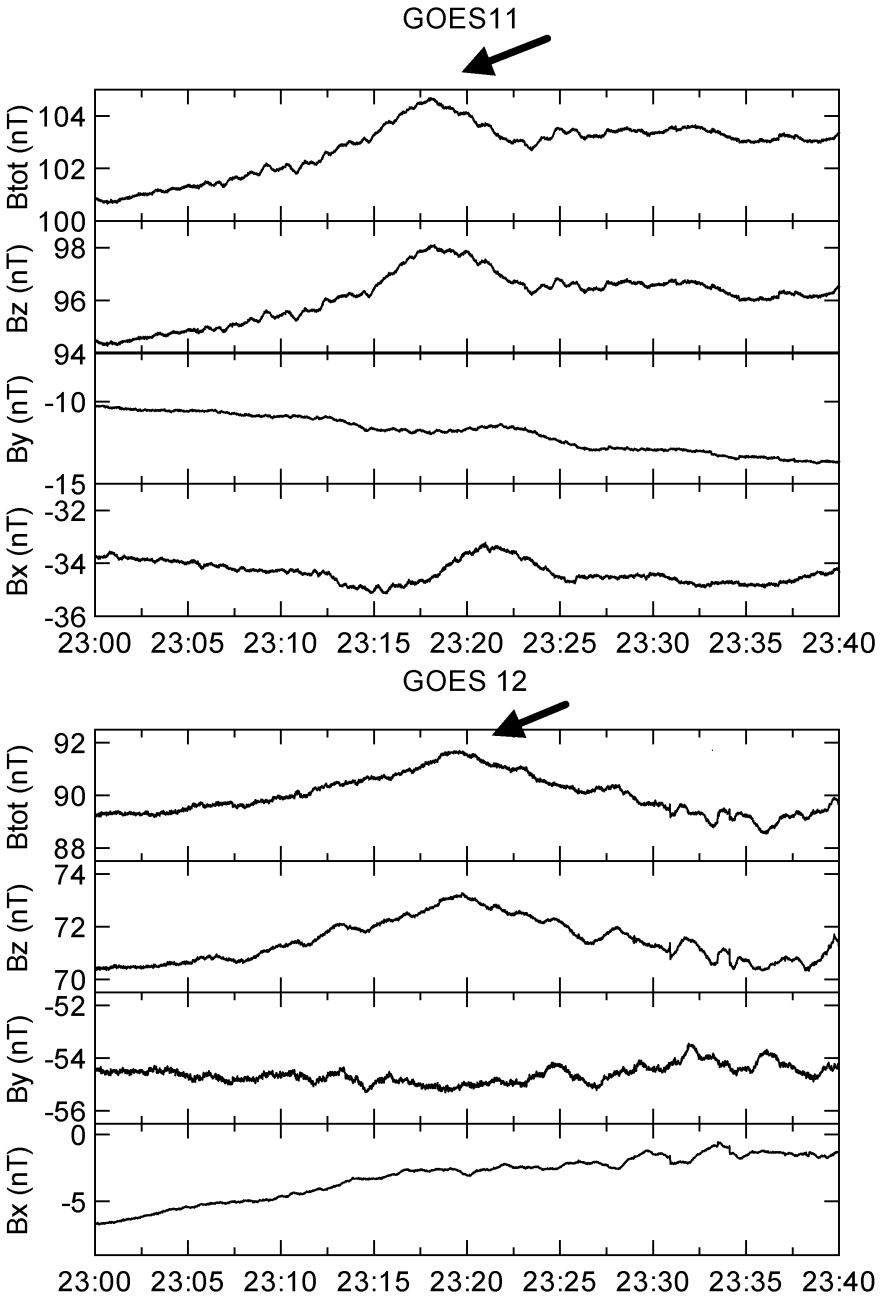

626

627 Fig.3. GOES 11 and GOES 12 magnetic field observations in GSM coordinates from
628 2300 UT to 2340 UT on October 15, 2008. Arrows show a compression of the
629 magnetosphere.

630

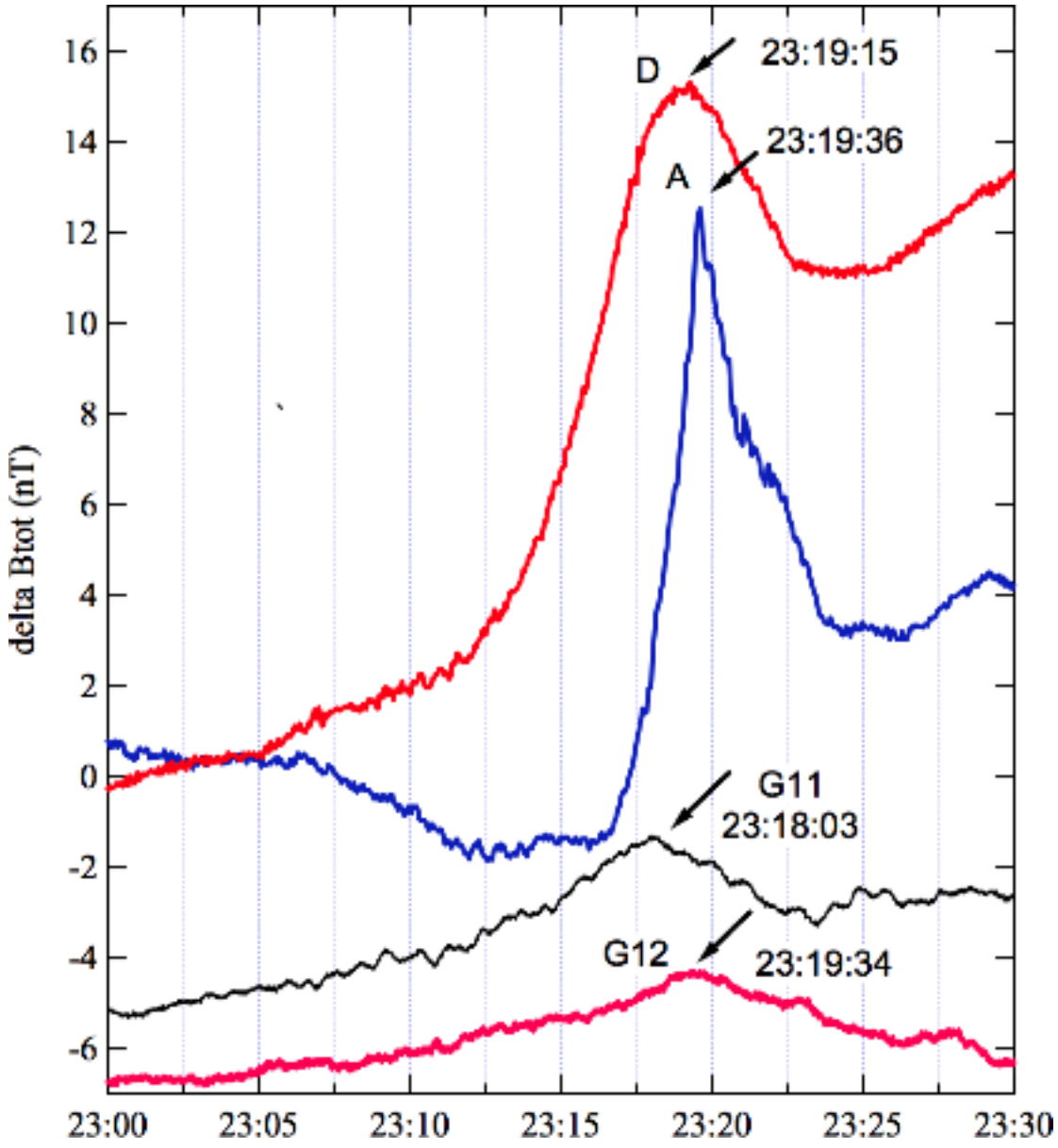

631

632

633 **Fig. 4. Variations in the total magnetic field strength observed by GOES-11 and -**

634 **12, THEMIS A and D from 2300 to 2330 UT on October 15, 2008. A constant value**

635 **has been subtracted from each trace so that they can be graphed on the same scale.**

636

637

638

639

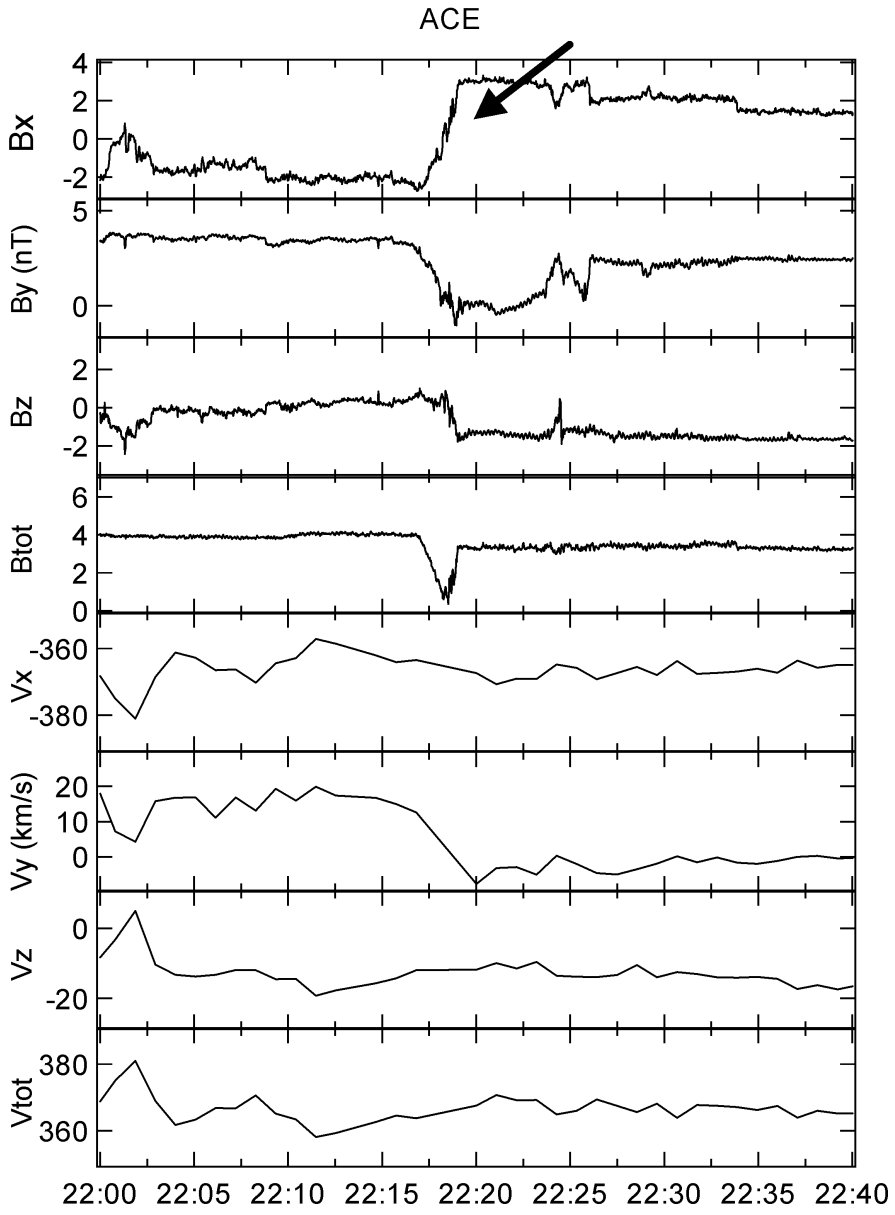

640

641 Fig. 5 ACE observations of the magnetic field and velocity in GSM coordinates from

642 2200 UT to 2240 UT on October 15, 2008. The arrow indicates a discontinuity.

643

644

645

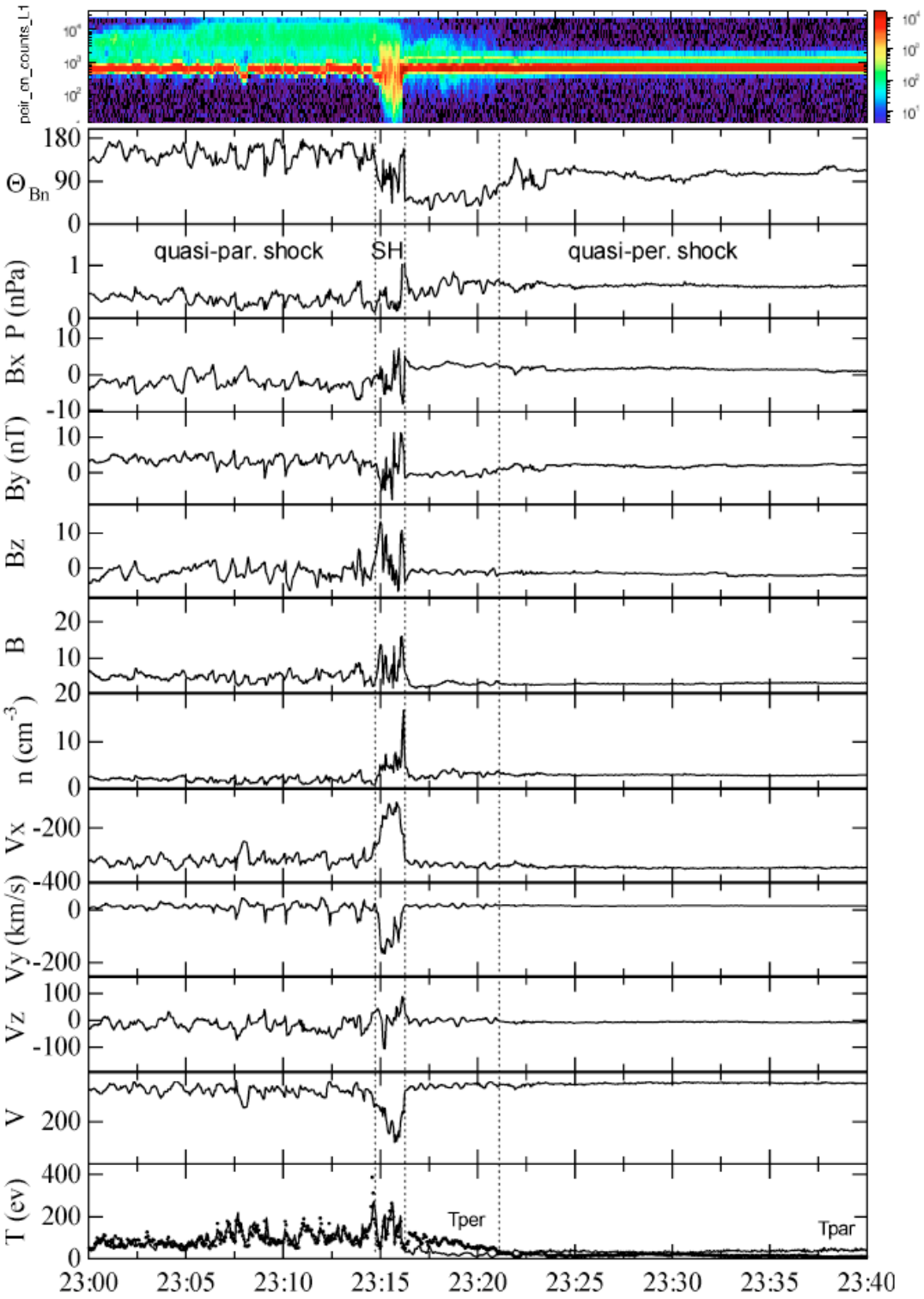
poir_en_counts_L1
Θ Bn
quasi-par. shock
SH
quasi-per. shock
P (nPa)
Bx
By (nT)
Bz
B
n (cm-3)
Vx
Vy (km/s)
Vz
V
T (ev)
Tper
Tpar
23:00
23:05
23:10
23:15
23:20
23:25
23:30
23:35
23:40

646

647

648

649

650 Fig. 6. THEMIS C observations of ion energy spectra, plasma and magnetic field from
651 2300 UT to 2340 UT on October 15, 2008. From top to bottom, the panels show the flux
652 spectrogram for ions in the range of energies from 2 eV to 25 keV (ESA), **Θ_{Bn}, the angle**
653 **between the magnetic field and the local bow shock normal, dynamic pressure, Bx,**
654 **By, Bz components of magnetic field in GSM coordinates and total magnetic field,**
655 **the ion density, the velocities in GSM coordinates, the ion temperatures**
656 **perpendicular and parallel to magnetic field. The spacecraft began the interval in**
657 **the quasi-parallel foreshock ($\Theta_{Bn} < 45°$). Two vertical dashed lines bound a brief**
658 **period in the magnetosheath. Upon exiting the magnetosheath, the spacecraft was**
659 **in a transitional region between the quasi-parallel and quasi-perpendicular**
660 **foreshock ($\Theta_{Bn} \sim 45°$). The third vertical dashed line marks the transition to the**
661 **quasi-perpendicular bow shock ($\Theta_{Bn} > 45°$).**

662

663

664

665

666

667

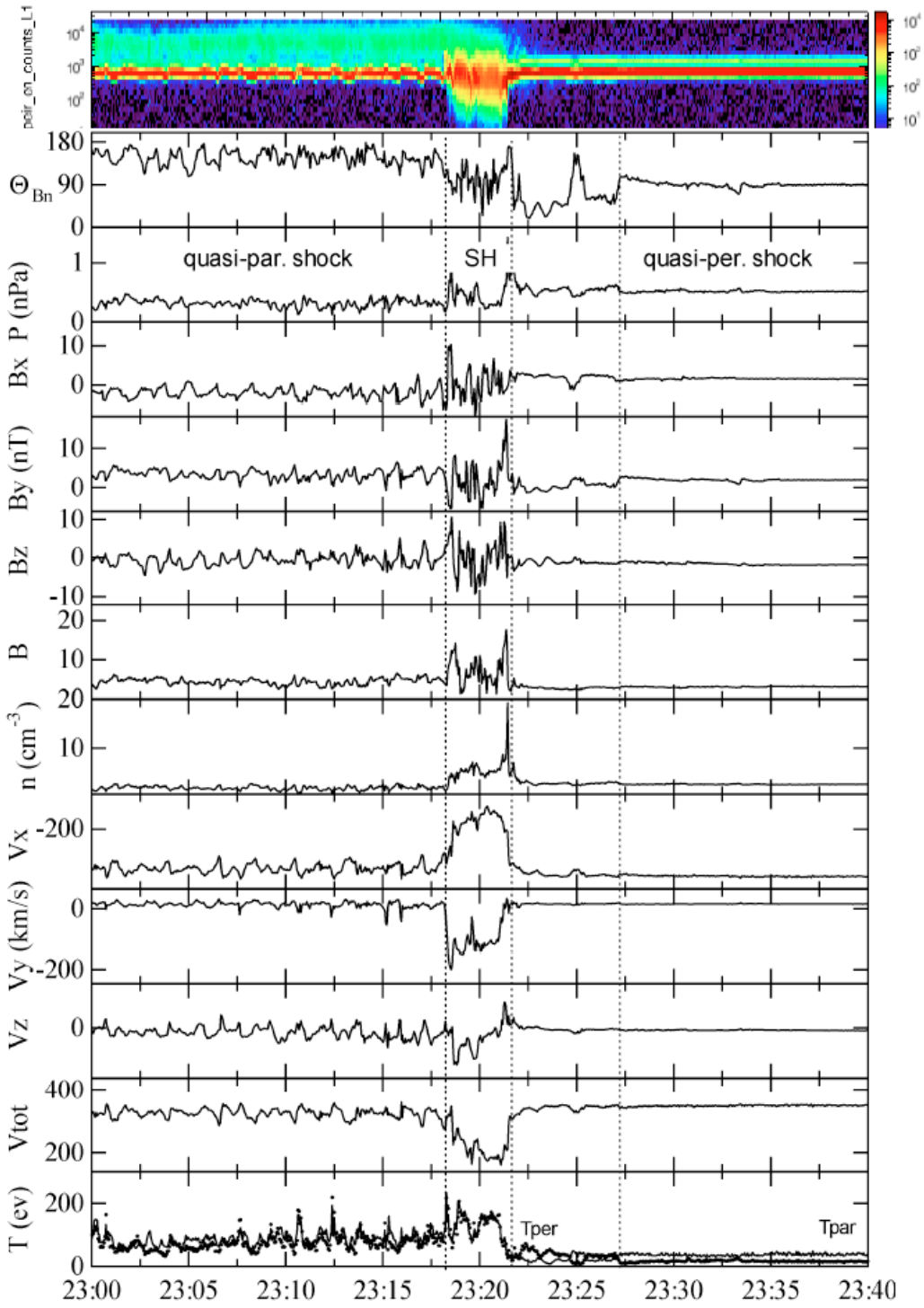

668

669

670 Fig. 7. The same as for Fig. 6 except for THEMIS B observations.

671

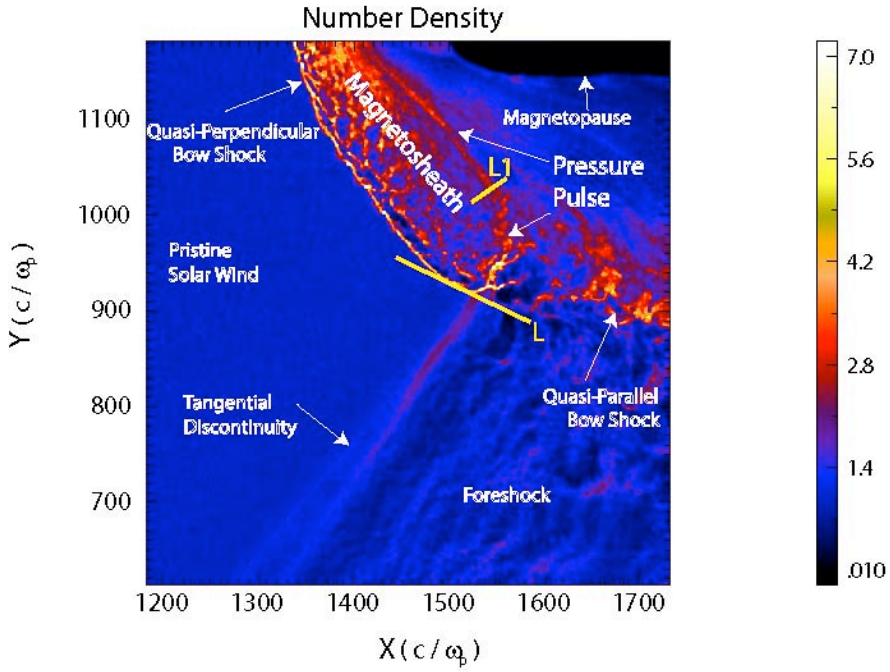

Fig. 8. Color intensity plot of density in the run for a portion of the simulation box (noon-midnight meridian plane) containing the dayside and post-noon bow shock. The density is normalized to the solar wind density, X points antisunward and Y points northward.

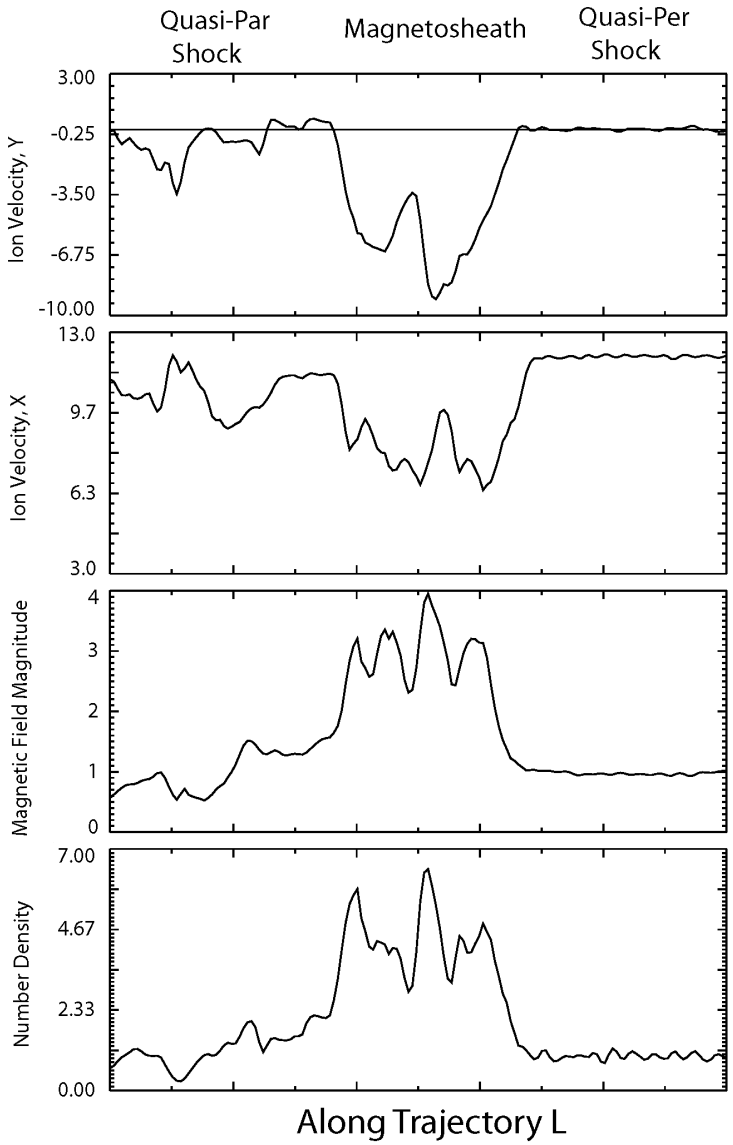

682

683 Fig.9. Snapshots of ion Vx and Vy velocities, magnetic field strength, and density along
684 the cut labeled "L" in Figure 8. Velocities are normalized to the Alfvén speed in the solar
685 wind while the magnetic field and density are normalized to their corresponding values in
686 the solar wind.

687

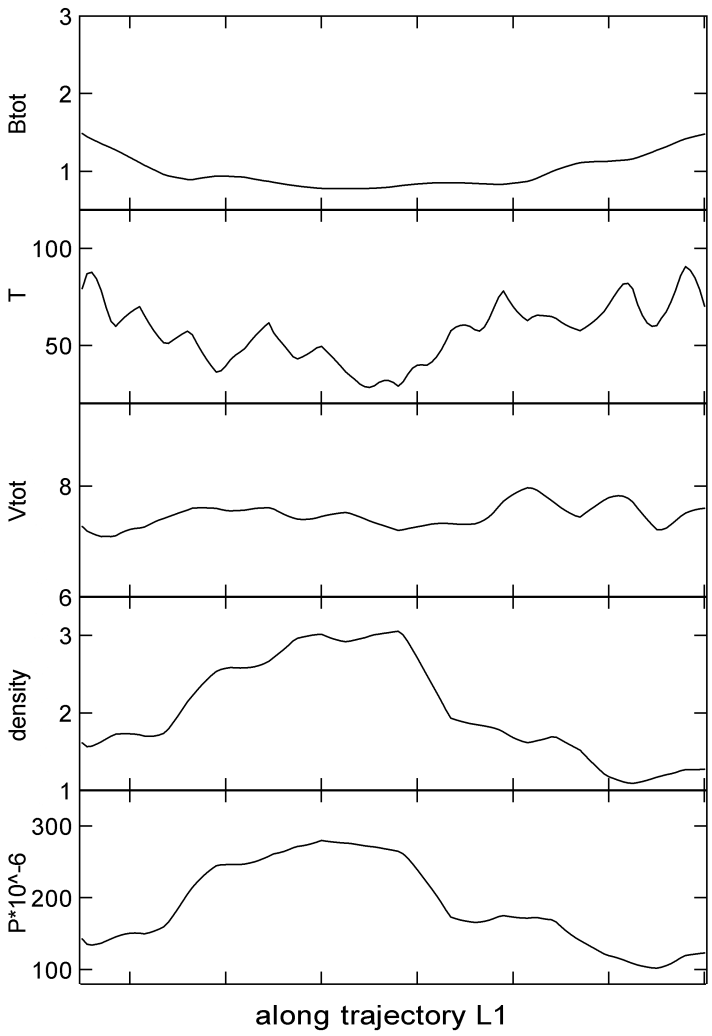

688

689 Fig.10. Snapshots of magnetic field strength, temperature, magnitude of the ion velocity,
690 density and dynamic pressure along the cut labeled "L1" in Figure 8. Velocity is
691 normalized to the Alfvén speed in the solar wind while the magnetic field and density are
692 normalized to their corresponding values in the solar wind.

693

694

695

696

697

698

699

700

701